Disordered atomic column state in Fe-Mo alloys

A. Hirata
The Institute of Scientific and Industrial Research, Osaka University, Ibaraki, Osaka 567-0047, Japan

Y. Koyama
Kagami Memorial Laboratory for Materials Science and Technology and Department of Materials Science and Engineering, Waseda University, Shinjuku, Tokyo 169-0051, Japan

(Received 20 November 2003; published 12 October 2004)

Changes in crystallographic features during the (bcc→bcc+*C*14 structure) reaction have been investigated for Fe-Mo alloys containing around 10 at. % Mo by transmission electron microscopy. The metastable bcc Fe-Mo alloys were annealed at the relatively low temperature of 1023 K in order to elucidate the details of the structural change in the initial stage. The annealing led to the appearance of precipitates in the bcc matrix, which did not have the *C*14 structure even after 1000 h of annealing. The structure of the precipitate was basically characterized by a disordered arrangement of distorted decagonal columns. The column was composed of distorted icosahedral clusters connected one-dimensionally. In addition, annealing was found to cause an increase in the number of *C*14 configurations for the local arrangement of these decagonal columns.

DOI: 10.1103/PhysRevB.70.134203 PACS number(s): 61.66.Dk, 68.37.Lp

I. INTRODUCTION

Among various crystal structures, there exist the crystal structures in the Laves phases, which are characterized by the arrangement of 12- and 16-fold-coordination polyhedra.[1,2] Between these two types, the 12-fold-coordination polyhedra can be regarded as a distorted icosahedral cluster. Recently, the tetrahedron involved in the 12-fold-coordination polyhedron was found to have a covalent nature.[3,4] That is, a three-dimensional network of covalent bonds has been found in the Laves structures. Our interest in this system is focused on how the covalent network is formed from the metallic structure. In order to answer this question, we have investigated the formation of two typical Laves structures, that is, the *hP*-12 $MgZn_2$-type and *cF*-24 $MgCu_2$-type structures, called the *C*14 and *C*15 structures, respectively. As for the *C*15 structure, we already reported the appearance of the icosahedral atomic cluster with the local covalent bonds during the bcc→*C*15 structural change in Ti-Cr alloys.[5] In the present work, we focus on the *C*14 structure in Fe-Mo alloys.

According to the reported phase diagram of Fe-Mo alloy system,[6] the (bcc→bcc+*C*14) reaction is expected below 1200 K in Fe-Mo alloys with a Mo composition of around 10 at. %. In order to understand the formation of the *C*14 structure, we annealed the metastable bcc alloys around 10 at. % Mo at the relatively low temperature of 1023 K. Low-temperature annealing was adopted to allow a slow reaction for obtaining each step in the initial structural change. Although precipitates were found in the bcc matrix, observations made by transmission electron microscopy indicated that the slow reaction at 1023 K never led to the equilibrium *C*14 phase, even after 1000 h of annealing. The crystal structure of the precipitate was characterized by a disordered arrangement of distorted decagonal columns with a column axis along the $[1\bar{1}0]_B$ direction. Note that the subscript *B* denotes the bcc structure. In this paper, we describe and analyze experimental results obtained in the reaction of the Fe-Mo alloys. It should be noted that, although several studies on the reaction have been performed,[7–11] the detailed change in the atomic arrangement for the formation of the *C*14 structure compared to that of bcc is not yet fully understood.

II. EXPERIMENTAL PROCEDURE

Ingots of Fe-Mo alloys containing around 10 at. % Mo were made from Fe (99.9%) and Mo (purity 99.9%) by the Ar-arc-melting technique. The ingots were annealed at 1473 K for 2 h for solution treatment. Samples were cut from the quenched ingot and annealed at 1023 K for 5 min, 30 min, 100 h, and 1000 h respectively, followed by quenching in ice water. Residual oxygen involved in the samples may play a role in the formation of the intermediate phase, particularly the quasicrystal, which consists of icosahedral atomic clusters.[12] Annealing was then performed under vacuum conditions of about 3.0×10^{-5} torr. The electron-energy-loss spectroscope (EELS) measurement confirmed that there was no signal due to oxygen atoms.

The samples were observed using a JEM-3010 (300 kV) transmission electron microscope at room temperature. The Ar-ion thinning technique was used to prepare specimens for observations. Among the alloys examined in the present work, we here describe the experimental data obtained from the Fe–10 at. % Mo alloy. This is because the experimental data of the Fe–10 at. % Mo alloy are the same as those of the others.

As an aid to the understanding of our experimental and analyzed results, we briefly summarize the crystallographic features of the equilibrium *C*14 structure. Figure 1 depicts the $[11\cdot0]_C$ projection of the *C*14 structure and the corresponding calculated diffraction pattern, together with a schematic diagram of the distorted decagonal atomic columns involved in it. The subscript *C* denotes the *C*14 structure. In

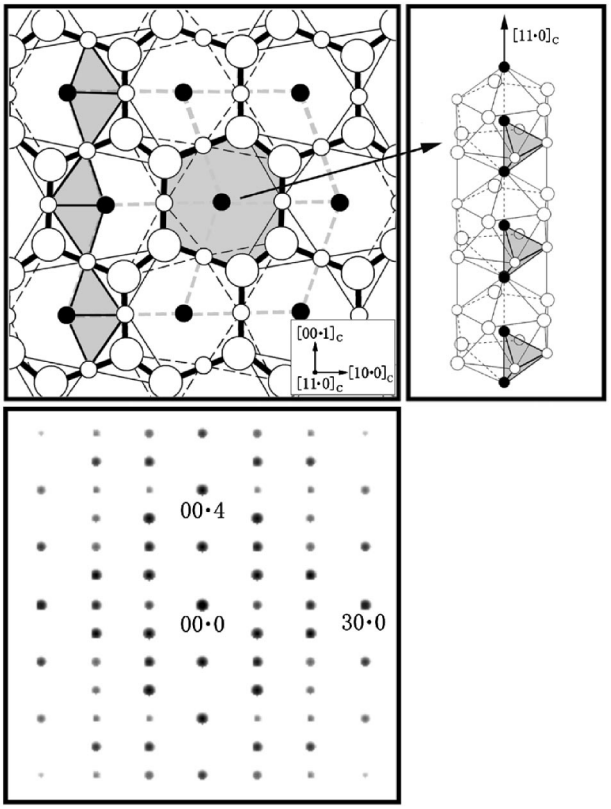

FIG. 1. Schematic diagram of $[11\cdot0]_C$ projection, together with a distorted decagonal atomic column. Covalent tetrahedra are depicted by the gray regions in both figures. The corresponding calculated diffraction pattern of the $C14$ structure is also shown in the lower part of the figure.

the figure, small and large circles indicate the Fe and Mo atoms, respectively. The atoms shown by open and closed circles are situated at $z=0$ or $1/2$ and at $z=1/4$ and $3/4$, respectively. The z direction is parallel to the $[11\cdot0]_C$ direction. The covalent tetrahedra consisting of four majority Fe atoms are also shown by the dark gray regions in both the projection and the diagram. Note that, according to the structural data reported by Sinha *et al.*,[6] the covalent bond length in the tetrahedron was calculated to be about 0.237 nm. In the upper right diagram, the distorted decagonal column is characterized by a one-dimensional array of 12-fold-coordination polyhedra; that is, the distorted icosahedral clusters, along the $[11\cdot0]_C$ direction. The $C14$ structure can then be regarded as the ordered state of these decagonal columns, which are indicated by the thick solid lines in the projection. The characteristic feature of the decagonal-column arrangement in the $C14$ structure is that the centers of the four neighboring columns are located so as to form a rhomboid tile, denoted by the thick dotted lines. From these structural features, ten strong reflections indicated by the arrows in the diffraction pattern are arranged with pseudodecagonal symmetry, as is shown in the lower diagram.

III. EXPERIMENTAL RESULTS

In the present work, a relatively low-temperature annealing at 1023 K for the Fe–10 at. % Mo alloy was made to obtain each step in the initial stage of the (bcc→bcc+$C14$) reaction. Precipitates were found to appear in all samples annealed for 5 min, 30 min, 100 h, and 1000 h. A bright field image exhibiting the precipitates in the 30-min annealed sample is, as an example, shown in Fig. 2. The electron incidence of the image is parallel to the $[1\bar{1}0]_B$ direction of the bcc matrix. In the image, we see the precipitates having various sizes, which are observed as a rather uniform region of lower contrast in the bcc matrix. The size of the precipitate indicated by the arrow is, for instance, estimated to be about 300 nm in length and about 50 nm in width. In addition, rotation of the sample indicated that every precipitate has a platelike shape with the normal direction parallel to one of the $\langle110\rangle_B$ directions. It should further be noted that the microstructure shown in Fig. 2 is basically the same as those in the other samples with different annealing times. Concretely, the size of the precipitates was almost unchanged in the annealing in spite of their increasing numbers. We believe that this change in the annealing is a characteristic feature of the initial stage of the (bcc→bcc+$C14$) reaction in the Fe-Mo alloys, as has been discussed by Hornbogen.[8]

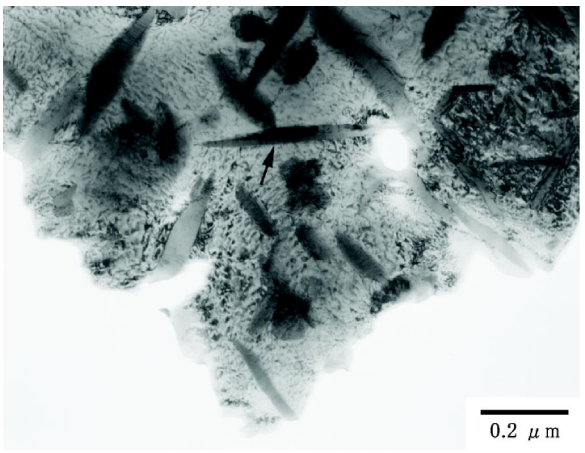

FIG. 2. Bright field image taken from the 30-min annealed sample. Electron incidence is parallel to the $[1\bar{1}0]_B$ direction.

The characteristic change in electron diffraction patterns of the precipitate formed during annealing was found in the $[1\bar{1}0]_B$ incidence for the bcc matrix. Figures 3(a)–3(c) are, respectively, three $[1\bar{1}0]_B$ diffraction patterns of the precipitates in the samples annealed for 5 min, 30 min, and 1000 h. In the (a) pattern of the precipitate in the 5-min annealed sample, there are many reflections with weak intensities, in addition to the strong reflections due to the bcc matrix. The notable feature of the weak reflections is that, in two scattering-angle regions of $\sin\theta/\lambda=(0.21\ \text{nm})^{-1}$ and $(0.13\ \text{nm})^{-1}$, ten pairs of two reflections indicated by ten double arrows are arranged with a pseudodecagonal symmetry with respect to the origin 000, although two of the ten reflections around the former $\sin\theta/\lambda=(0.21\ \text{nm})^{-1}$ are located at the same positions of the 110_B and $\bar{1}\bar{1}0_B$ bcc reflections. In the 30-min annealed sample of (b), these 20 reflections are present with strong intensities, together with the appearance of new weak reflections, as is indicated by ar-

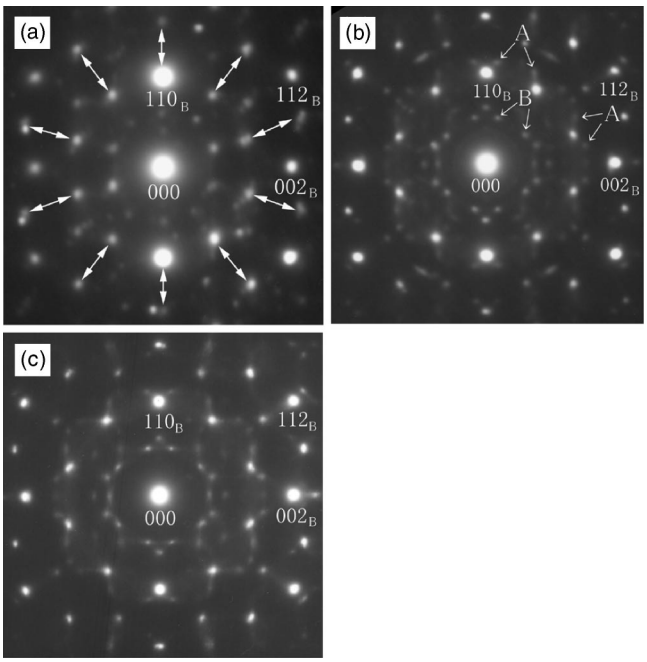

FIG. 3. Electron diffraction patterns taken from samples annealed (a) 5 min, (b) 30 min, and (c) 1000 h. Electron incidences of (a), (b), and (c) are parallel to the $[1\bar{1}0]_B$ direction.

rows *A* and *B*. The reflections *A* and *B* are further found to become sharp in the 1000-h annealed sample, but the (c) pattern cannot be identified as the *C*14 pattern. In spite of no *C*14 pattern, this change in the patterns suggests that the structural change in the precipitate occurs in two steps. That is, the first step (FS) is characterized by the appearance of reflections with the pseudodecagonal-symmetry arrangement, while second step (SS) brings about the reflections *A* and *B*. These two sets of reflections, respectively, are referred to as FS and SS reflections in this paper.

As was mentioned above, the FS reflections characterizing the first step have only weak intensities in the 5-min annealed sample. We examined the position of the FS reflections with the strong intensities in reciprocal space, using the 30-min annealed sample, in spite of the presence of weak SS reflections in the second step. Figure 4 shows a series of electron diffraction patterns taken from the precipitate in the sample annealed for 30 min at 1023 K, together with a schematic diagram of the decagonal atomic column and its projection along the column axis. Six important electron diffraction patterns of the precipitate are arranged in the stereographic projection in order to understand the orientation relationship among these six patterns. The electron incidence of each pattern is indexed in terms of the bcc matrix. In the stereographic projection, the $[1\bar{1}0]_B$ pattern in Fig. 4(a) is the same as that in Fig. 3(b) and exhibits the pseudodecagonal symmetry for the strong FS reflections. As for the other patterns, the pseudodecagonal arrangement of the strong FS reflections is also seen in the $[\bar{1}13]_B$ pattern, as is indicated by the ten arrows in Fig. 4(b). The patterns in (c), (d), (e), and (f) are, on the other hand, found to show the twofold arrangement of the strong FS reflections, together with the presence of streaks through the reflections. Careful examination of these four patterns indicates that they can be classified into two groups, that is, the patterns in (c) and (d), and those in (e) and (f). The difference between these two groups is that in the case of (e) and (f), for instance, the reflections are present in the interior of the regions surrounded by the white lines. We then tried to construct an atomic-arrangement model consistent with the features of the diffraction patterns. It turned out to be indicative of the appearance of the pseudodecagonal atomic column, which is depicted in the center part of the stereographic projection. The electron incidences of these patterns are also shown by the arrows in the schematic diagram of the column and the projection. Surprisingly, the angles among the electron incidences are, within the experimental error, the same as those expected from the ideal decagonal column. We conclude that in the low-temperature annealing at 1023 K, the formation of the decagonal atomic column occurs in the first step of the structural change from the bcc structure.

The second step in the structural change is the appearance of the SS reflections. Because the *B* reflections are particularly observed in the relatively low-scattering-angle region, $\sin\theta/\lambda = (0.35\ \text{nm})^{-1}$, in the $[1\bar{1}0]_B$ pattern, the SS reflections would reflect the neighboring arrangement of the decagonal atomic columns. In order to elucidate the arrangement, we took high-resolution micrographs of precipitates found in both the 30-min and 1000-h annealed samples. It was difficult to find any difference between these samples in the micrographs, although the spatial configuration analysis of the columns gave us a certain difference, as will be mentioned later.

Figure 5 shows micrographs obtained from the 30-min annealed sample. Two high-resolution micrographs of the same precipitate in the sample are given in Fig. 5(a), together with their corresponding electron diffraction patterns. The electron incidences of the micrographs in (a) and (b) were, respectively, parallel and perpendicular to the $[1\bar{1}0]_B$ direction along the column axis. The sample thickness was evaluated to be about 10 nm in both images, while the magnitude of the defocus used was about −100 nm for (a) and about −60 nm for (b). In the micrograph with the incidence parallel to the column axis in (a), many bright dots are observed in the whole area. The average distance between two neighboring dots is estimated to be about 0.35 nm, but there appears to be no regular arrangement of the dots. Note that, as will be described later, each dot represents the center of a decagonal column. Based on this analysis, the arrangement of the columns should be characterized by only their short-range ordering. In order to confirm this result, we look at the micrograph with the incidence perpendicular to the column axis in (b). Only a one-dimensional array of the bright dots can be seen along the $[1\bar{1}0]_B$ direction, as is shown by the white arrows in the micrograph. If the column arrangement had a long-range character, on the other hand, a two-dimensional regular array of the bright dots would be observed in this micrograph. It is thus understood that, although the decagonal columns are formed with the column axis along the $[1\bar{1}0]_B$ direction, a long-range ordering of their arrangement does not occur even in the 1000-h annealed sample.

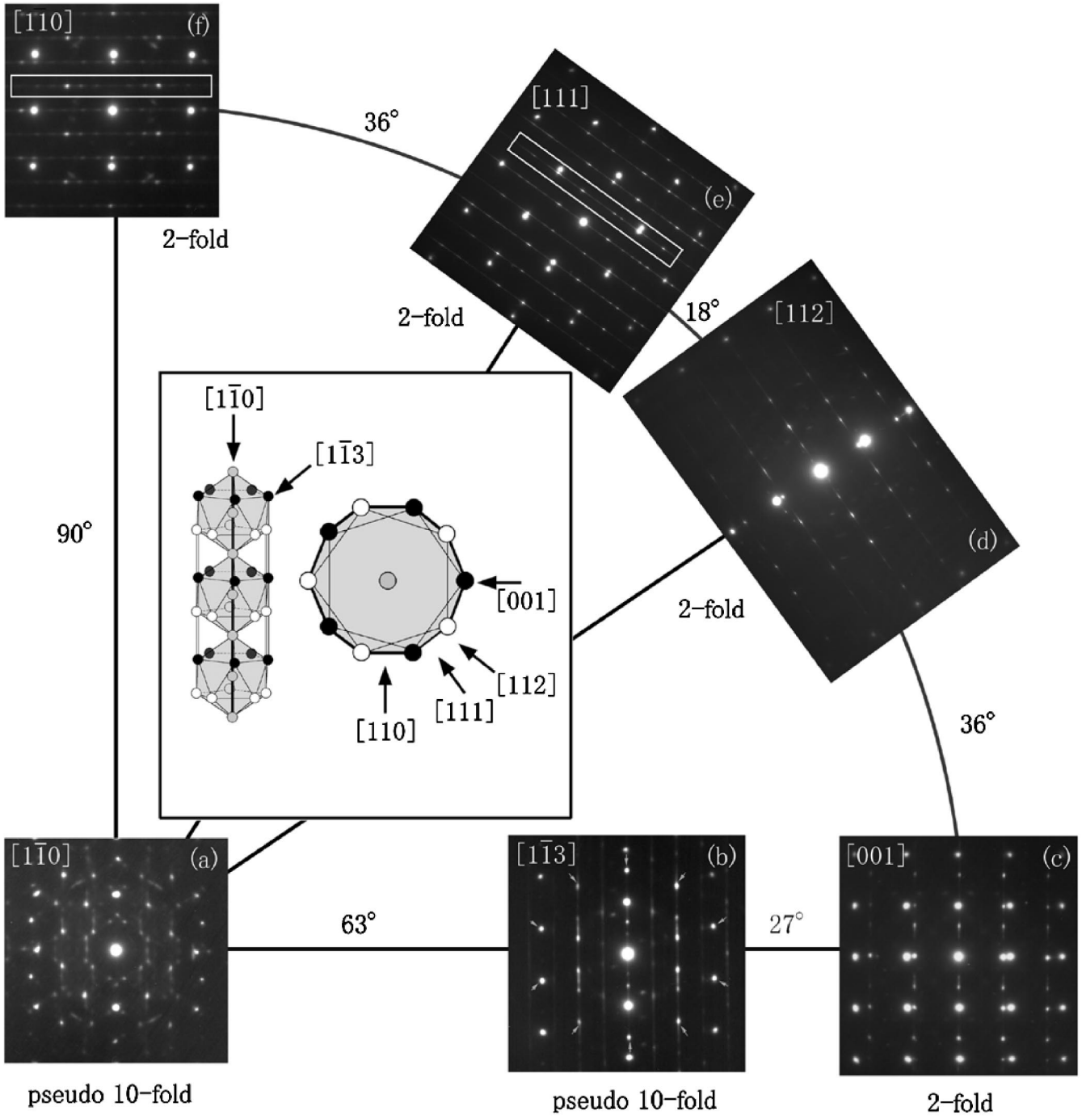

FIG. 4. Series of diffraction patterns obtained from the platelike precipitate in Fig. 2. Electron incidences of (a), (b), (c), (d), (e), and (f) are parallel to the $[1\bar{1}0]_B$, $[11\bar{3}]_B$, $[001]_B$, $[112]_B$, $[111]_B$, and $[110]_B$ directions, respectively.

IV. DETERMINATION OF THE ATOMIC ARRANGEMENT IN THE PRECIPITATES

In order to elucidate the detailed features of the column arrangement, we tried to determine the atomic positions in the precipitate. The positions of the atoms in the samples annealed for 30 min and 1000 h were analyzed by constructing the atomic-arrangement model consistent with their high-resolution micrographs and corresponding diffraction patterns. As the determined arrangements were basically the same in both samples, we here show the analyzed results for the 30 min annealed sample in Fig. 6. Figures 6(a)–6(d) are, respectively, an enlargement of the area in the micrograph of Fig. 5(a) denoted by the white square, the $[1\bar{1}0]_B$ projection of the atomic-arrangement model, the calculated micrograph of the model, and the experimental and calculated diffraction patterns. The electron incidence in this case was parallel to the $[1\bar{1}0]_B$ column axis. In the projection of the model, the projected positions of one centered and ten surrounding at-

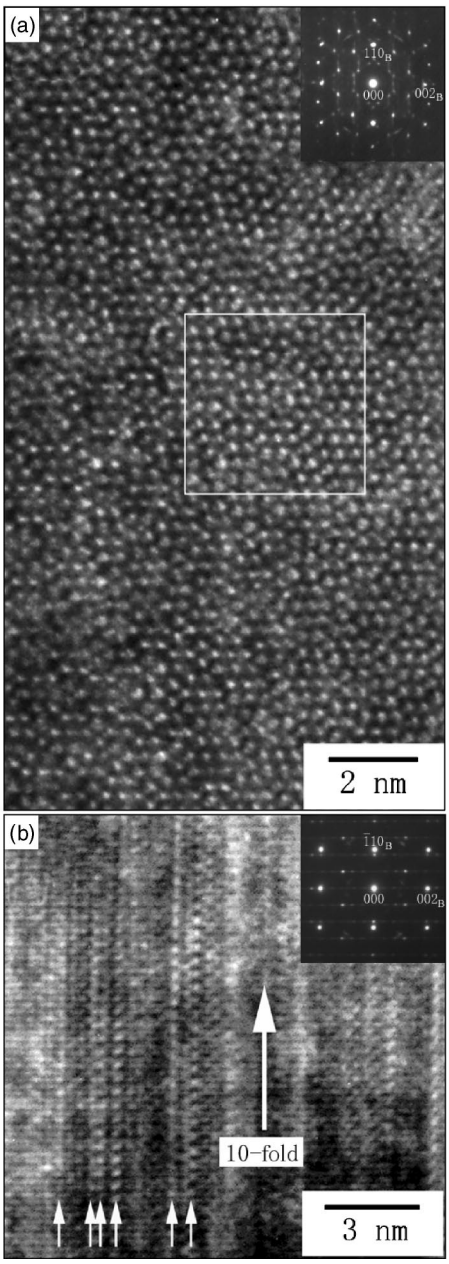

FIG. 5. High-resolution electron micrographs of the plate-like precipitate in the 30-min annealed sample with (a) $[1\bar{1}0]_B$ and (b) $[110]_B$ incidences, together with the corresponding electron diffraction patterns.

oms in each column are, respectively, denoted by the closed and open small circles, and those of the ten atoms are connected by the thin solid lines in order to show the shape of the decagonal column. The neighboring centered atoms are also connected by thick lines to better visualize the column arrangement. The calculated micrograph used a defocus of −100 nm and a specimen thickness of 10 nm. It was found that the calculated micrograph in Fig. 6(c) produced white dots, the positions of which were exactly the same as both those of the bright dots in Fig. 6(a) and those of the closed circles in Fig. 6(b). This agreement clearly indicates that each bright dot represents the center of a decagonal column,

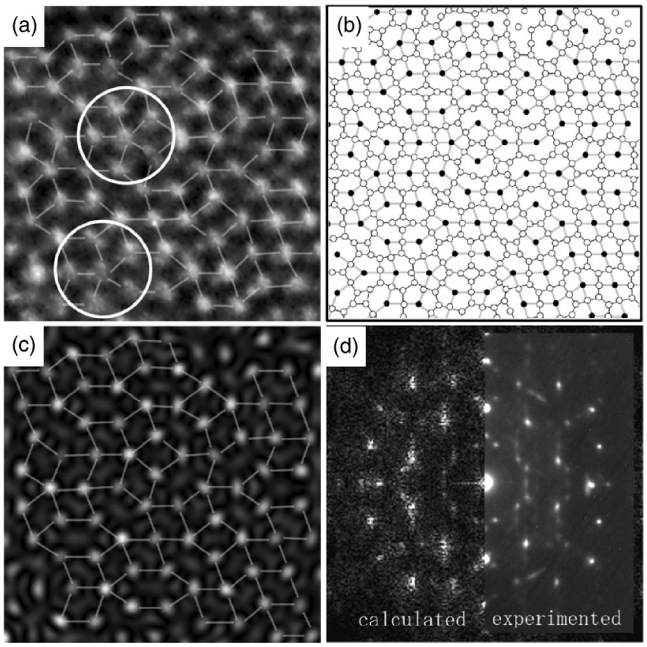

FIG. 6. (a) High-resolution electron micrograph obtained from the 30-min annealed sample, together with (b) a structural model of the corresponding region. The micrograph is an enlargement of the region enclosed by the white square in Fig. 5(a). In (c) and the left side of (d), the calculated micrograph and the Fourier-transformation pattern of the structural model are shown, respectively. In order to easily compare the Fourier-transformation pattern with the experimental one, the pattern in Fig. 5(b) is also shown in the right side of (d). The simulation of the micrograph was carried out under the conditions of −100-nm defocus and 10-nm thickness.

and that the array of columns is basically random. Furthermore, the $[1\bar{1}0]_B$ diffraction pattern for the model was calculated by its Fourier transformation to confirm the validity of the proposed arrangement. The calculated and experimental patterns are, respectively, shown on the left and right sides of Fig. 6(d). The calculated pattern well reproduces the major features of the experimental pattern even in the large scattering-angle region. The reproducibility confirms that the model is appropriate. Based on the model, a check of column shape reveals that they are not ideal decagonal prisms, which was suggested on the basis of the diffraction patterns in Fig. 4. This implies that the ideal decagonal column is just an average shape in a large area. The proposed model suggests that the atomic arrangement in the precipitate is basically characterized by a disordered array of the distorted decagonal columns having different shapes.

Although the $C14$ structure as an ordered structure of the columns was not obtained, some change in the local arrangement of columns in the precipitate appeared during the second step of the annealing process. In order to understand the annealing effect, the local arrangement of the columns in the 30-min and 1000-h annealed samples were analyzed on the basis of the determined atomic positions. In particular, we focused on the spatial configuration of neighboring columns around a centered column. This is because the SS reflections in the second step, particularly the B reflections, appear around $\sin\theta/\lambda = (0.35\ \text{nm})^{-1}$, the inverse of which almost

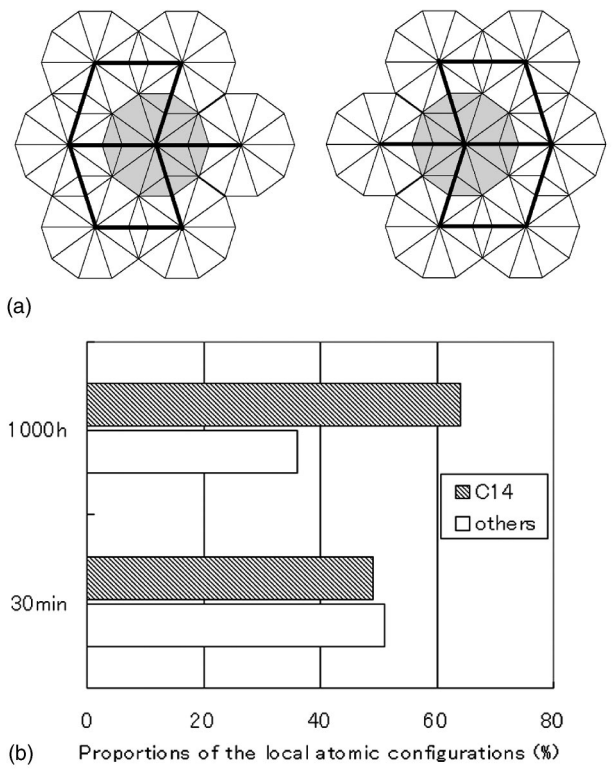

FIG. 7. (a) Two *C*14-type local configurations of the columns. (b) Proportions of the local configuration of 30-min and 1000-h annealed samples.

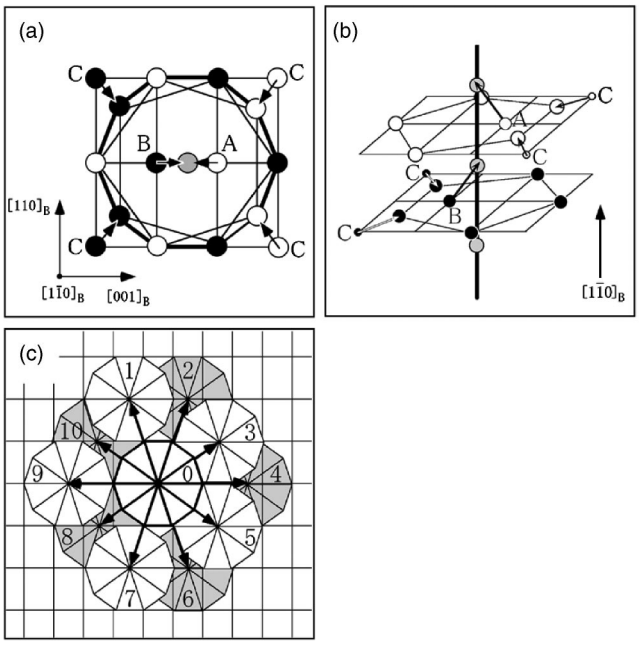

FIG. 8. (a) Two-dimensional and (b) three-dimensional diagrams of determined displacement from the bcc structure for the formation of a pseudodecagonal column. Ten possible positions of the neighboring atomic column are shown in (c).

corresponds to the distance between two neighboring columns. Two configurations in the *C*14 structure are depicted in Fig. 7(a). In the case of the 30-min annealed sample in Fig. 6(a), for instance, the centered column is surrounded by five neighboring columns, as is shown inside the white large circles. This configuration is different from that of the *C*14 structure in Fig. 7(a). We then counted the number of the *C*14 configurations in the atomic-arrangement models, although the determined model for the 1000-h annealed sample is not shown in this paper. In the count, configurations lacking one of the six neighboring columns in Fig. 7(a) were also regarded as a *C*14 configuration. The results for 200 configurations in the 30-min and 1000-h annealed samples are shown in Fig. 7(b). From the figures, it can be seen that the number of *C*14 configurations in the 1000-h annealed sample is slightly larger than that in the 30-min annealed sample. It thus seems that annealing at 1023 K statistically results in a tendency toward increasing the *C*14 configurations.

V. DISCUSSION

Based on both the experimental data and the analyzed results obtained in this study, we first propose an atomic-displacement model for the formation of the decagonal column. In addition, the stability of the decagonal column is also discussed in terms of the formation of covalent bonds in alloys.

The decagonal atomic column is directly formed from the bcc structure in the first step of the structural change. The electron diffraction patterns arranged on the stereograph in Fig. 4 clearly indicated that there is a specific orientation relationship between the bcc structure and the decagonal column. For example, the column axis was found to be parallel to the $[1\bar{1}0]_B$ direction. Based on this relationship, we proposed the atomic displacement for column formation from the bcc structure. The $[1\bar{1}0]_B$ projection of the displacement proposed here is depicted in Fig. 8(a), together with its three-dimensional diagram. As shown in these figures, the shifts of the atoms are simple and small. In particular, the atoms denoted by *A* and *B* are displaced to the middle positions on the column axis between two neighboring $(1\bar{1}0)_B$ planes. The atoms by *C* are, on the other hand, shifted only in the $(1\bar{1}0)_B$ planes to form the pentagonal arrangement. As a result of these shifts, the 12-fold-coordination polyhedron is formed, but is severely compressed along the $[1\bar{1}0]_B$ column axis. The distance between the *A* and *B* atoms along the column axis was estimated to be about 0.237 nm from the diffraction patterns in Fig. 4. Interestingly, this distance is exactly identical to that between the Fe atoms in the covalent tetrahedron for the *C*14 structure, as was mentioned earlier. The spatial configurations of the columns, which are predicted from this atomic displacement, are further depicted in Fig. 8(c). There are ten possible positions of the columns (numbered 1 through 10 in the figure) for the neighboring columns around the centered column, denoted by 0. Because of the volume of the column, it is obvious that all neighboring columns cannot be formed at the same time. A set of the neighboring columns such as the 1, 3, 5, 7, and 9 columns and the 1, 3, 5, and 8 columns are then possible as a spatial configuration. Note that these possible configurations are not identical to

the $C14$ configuration, but that the 1, 3, 5, 7, and 9 configuration is, for instance, seen in the atomic arrangement of the 30-min annealed sample, Fig. 6(b). This supports our atomic-displacement model as appropriate for the short-range column arrangement found experimentally. Thus, the subsequent annealing should lead to conversion to the $C14$ configurations. However, only a tendency for an increase in the number of $C14$ configurations was suggested in the present analysis.

The physical origin of the formation of the distorted decagonal column in the low-temperature annealing is now considered. As was mentioned earlier, the $C14$ structure is characterized by a three-dimensional network of the covalent tetrahedra composed of four small, majority Fe atoms. In the present study on the (bcc$\rightarrow$bcc+$C14$) reaction in Fe-Mo alloys, on the other hand, the distorted decagonal column was first formed in the annealing. This clearly suggests that the development of the network of covalent bonds should involve some steps in the structural change. In order to understand the physics of the decagonal-column formation in the development of the covalent bond, we examined the crystallographic features of the column, which is shown in both the inset of Fig. 4 and Fig. 6(b). The important feature of the column is that the shortest bond, with the length of about 0.237 nm, is present along the column axis. The length is the same as that between two neighboring Fe atoms in the covalent tetrahedron in Fig. 1. This presumably suggests that the appearance of the decagonal column results from the formation of the covalent chain along the column axis. Thus in the bcc$\rightarrow C14$ structural change, the covalent chain is formed in the first step of the development of the covalent bond. The conversion of the initial spatial configurations to the $C14$ configuration must then be associated with the local development of a coherent network of the covalent tetrahedra. On the other hand, judging by the lack of $C14$ structure, the three-dimensional regular network of the covalent tetrahedra is never developed in the present experimental condition, that is, the low temperature annealing at 1023 K.

Finally we briefly discuss the role of the Mo atoms in the decagonal-column formation. As was mentioned above, the appearance of the decagonal column is directly associated with the formation of the Fe-Fe covalent bonds along the column axis. It then seems that the Mo atoms occupying the surrounding positions of each columns do not play any role in the column formation. In order to form the covalent bond, however, it is necessary that charge transfer takes place between atomic species with different values for electronegativity.[13,14] That is, if the Mo atom is absent, the charge transfer cannot occur and the Fe-Fe covalent bond is not then formed. In this sense, the Mo atom is needed to form the decagonal column in the bcc$\rightarrow$bcc+$C14$ reaction.

VI. CONCLUSION

The purpose of our study, using low-temperature annealing of metastable bcc Fe-Mo alloys at 1023 K, is to elucidate which step is involved in the initial stage of the bcc$\rightarrow C14$ structural change. The present experimental data indicate that there are two steps in the initial stage. That is, the formation of the decagonal atomic column with a covalent chain along the column axis occurs in the first step. In the second step, the local arrangement of the decagonal columns tends to change into the $C14$ configuration. The change in the arrangement is presumably associated with the local development of a network of coherent covalent bonds. That is, the bcc$\rightarrow$bcc+$C14$ structural change in the Fe-Mo alloys is understood to start with the formation of the decagonal column with the covalent chain along the column axis.

ACKNOWLEDGMENT

The authors would like to thank Dr. Tanimura of Nissan ARC Ltd. for useful discussion.

[1] F. C. Frank and J. S. Kasper, Acta Crystallogr. **11**, 184 (1958).
[2] F. C. Frank and J. S. Kasper, Acta Crystallogr. **12**, 483 (1959).
[3] Y. Kubota, M. Takata, M. Sakata, T. Ohba, K. Kifune, and T. Tadaki, J. Phys.: Condens. Matter **12**, 1253 (2000).
[4] Y. Kubota, M. Takata, M. Sakata, T. Ohba, K. Kifune, and T. Tadaki, Jpn. J. Appl. Phys., Suppl. **38-1**, 456 (1999).
[5] A. Hirata, Y. Koyama, and M. Tanimura, Phys. Rev. B **67**, 144107 (2003).
[6] A. K. Sinha, R. A. Buckley, and W. Hume-Rothery, J. Iron Steel Inst., London **205**, 191 (1967).
[7] E. Hornbogen, J. Appl. Phys. **32**, 135 (1961).
[8] E. Hornbogen, Trans. Metall. Soc. AIME **227**, 1411 (1963).
[9] H. L. Marcus, M. E. Fine, and L. H. Schwartz, J. Appl. Phys. **38**, 4750 (1967).
[10] J. Higgins and P. Wilkes, Philos. Mag. **25**, 599 (1972).
[11] T. Miyazaki, S. Takagishi, H. Mori, and T. Kozakai, Acta Metall. **28**, 1143 (1980).
[12] J. L. Libbert and K. F. Kelton, Philos. Mag. Lett. **71**, 153 (1995).
[13] L. Pauling, *The Nature of the Chemical Bond* (Cornell University Press, Ithaca, NY, 1952).
[14] J. Hafner, J. Phys. F: Met. Phys. **15**, 1879 (1985).